NANO · MICRO small
www.small-journal.com

Impact of Surface Ligand on the Biocompatibility of InP/ZnS Quantum Dots with Platelets

Hélio M. Gil, Zoe Booth, Thomas W. Price, Jessica Lee, Leigh Naylor-Adamson, Michelle Avery, Alina Muravitskaya, Nicole Hondow, David Allsup, Jürgen E. Schneider, Khalid Naseem, Ali M. Adawi, Jean-Sebastien G. Bouillard, Thomas W. Chamberlain, Simon D. J. Calaminus, and Graeme J. Stasiuk**

InP/ZnS quantum dots (QDs) have received a large focus in recent years as a safer alternative to heavy metal-based QDs. Given their intrinsic fluorescent imaging capabilities, these QDs can be potentially relevant for in vivo platelet imaging. The InP/ZnS QDs are synthesized and their biocompatibility investigated through the use of different phase transfer agents. Analysis of platelet function indicates that platelet-QD interaction can occur at all concentrations and for all QD permutations tested. However, as the QD concentration increases, platelet aggregation is induced by QDs alone independent of natural platelet agonists. This study helps to define a range of concentrations and coatings (thioglycolic acid and penicillamine) that are biocompatible with platelet function. With this information, the platelet-QD interaction can be identified using multiple methods. Fluorescent lifetime imaging microscopy (FLIM) and confocal studies have shown QDs localize on the surface of the platelet toward the center while showing evidence of energy transfer within the QD population. It is believed that these findings are an important stepping point for the development of fluorescent probes for platelet imaging.

1. Introduction

Effective in vivo imaging of pathological thrombi has become a topic of significant interest in recent years. Thrombi are produced through the activation of a blood cell called the platelet and are formed to prevent excessive bleeding. However, in certain disease states, platelets can over-activate and therefore cause the formation of an excessively large thrombus. These thrombi can block blood vessels, either in the location where they are formed, or they can move and block blood vessels at a different location, leading to thrombotic diseases such as stroke, pulmonary emboli, and heart attacks.

The use of nanomaterial probes could prove to be a valuable option for improved imaging of thrombi. Numerous studies have employed nanoparticles as molecular imaging tools to image components

H. M. Gil, T. W. Price, G. J. Stasiuk
Department of Imaging Chemistry and Biology
School of Biomedical Engineering and Imaging Sciences
King's College London
London SE1 7EH, UK
E-mail: graeme.stasiuk@kcl.ac.uk

H. M. Gil, Z. Booth, L. Naylor-Adamson, D. Allsup, S. D. J. Calaminus
Centre for Biomedicine
Hull York Medical School
University of Hull
Hull HU6 7RX, UK
E-mail: simon.calaminus@hyms.ac.uk

J. Lee, M. Avery
Centre for Biomedicine
University of Hull
Hull HU6 7RX, UK

The ORCID identification number(s) for the author(s) of this article can be found under https://doi.org/10.1002/smll.202304881

DOI: 10.1002/smll.202304881

A. Muravitskaya, A. M. Adawi, J.-S. G. Bouillard
Department of Physics and Mathematics
University of Hull
Hull HU6 7RX, UK

N. Hondow
School of Chemical and Process Engineering
University of Leeds
Leeds LS2 9JT, UK

J. E. Schneider
School of Medicine
University of Leeds
Leeds LS2 9JT, UK

K. Naseem
Leeds Institute of Cardiovascular and Metabolic Medicine
University of Leeds
Leeds LS2 9JT, UK

T. W. Chamberlain
Institute of Process Research and Development
School of Chemistry
University of Leeds
Leeds LS2 9JT, UK

of a thrombus; from targeting the fibrin mesh by using a fibrin-targeting peptide attached to the surface of superparamagnetic nanoparticles,[1] to probing platelets themselves and monitoring platelet activity using titanium nitride nanocoatings.[2] Such developments could not only help aid our understanding of thrombus size and composition but also aid in the production of more effective thrombolytic agents and anticoagulant therapies. Subsequently, selecting a nanoparticle that itself possesses fluorescent properties would be a beneficial first step in developing a platelet-based imaging nanoparticle.

Consequentially, this research has focused on quantum dots (QDs), which are semiconductor nanocrystals that possess bright and tuneable emission and desirable physiochemical properties. QDs with a core/shell structure attract particular interest since these provide stable and efficient photoluminescence.[3] The core elements predominantly come from groups II–VI (CdSe, CdS), group IV (C, Si, Ge), and III–V (InP, GaP, GaN), whilst the shell is commonly composed of elements from the groups II–VI (ZnS, ZnSe).[4] There are also reports of QDs that use common core elements as shell material to achieve different photophysical properties.[5] In particular, for InP QDs, the action of shelling provides many benefits such as improving the quantum yield,[6–8] increasing the photostability of the QD, and preventing the core from oxidizing.[9–11] These photoluminescent qualities allow QDs to have many applications ranging from optoelectronic devices, such as solar harvesting and lighting, to biomedical imaging.[12,13] Independent of the material, the emission wavelength of QDs is size-dependent and can be tuned during synthesis.[4] For imaging applications, QDs have been prepared with emission wavelengths ranging from the visible to the near-infrared (NIR) range.[14] QDs have also been used as a platform for multimodal imaging with the incorporation of magnetic resonance imaging (MRI) agents and positron emission tomography (PET) tracers to enable multiple imaging options.[12,13,15–17] Since QDs are usually synthesized in organic media,[6,15] before they can be used for biological purposes, it is crucial to transfer QDs to the aqueous phase. This is typically achieved using thiol-containing hydrophilic ligands.[16,17] Formulations with these surface molecules have been reported using ligands such as thioglycolic acid (TGA),[17] penicillamine (Pen),[18] lipoic acid (LA),[19] or glutathione (GSH).[20]

There are however conflicting reports of the effect of QDs on the platelet with some indicating Cd- and C-based QDs can cause activation of the platelet, whilst some report inhibition of the platelet function.[21,22] There is no report on the effect of InP/ZnS QDs on platelet function. The rationale for investigating QD-platelet interactions is two-fold. Inhibition of platelet function by the QD could cause excessive bleeding, whilst activation of platelets, independent of natural agonists, could lead to the formation of a thrombus large enough to obstruct the flow of blood (pathological thrombus). Critical to the effect on platelets, and therefore the QD-platelet specific biotoxicity, is the concentration of the QDs, the core and shell materials used, and the ligands used for phase transfer of the nanoparticles.[23] Importantly, InP/ZnS QDs have been identified as a non-toxic alternative to Cd-based QDs by numerous studies within the literature both in vivo and in vitro.[24–26] However, the specific effects upon the platelet caused by both the QD materials and the ligands used to promote QD water dispersibility are unclear and need to be investigated. Therefore, determining how or if InP/ZnS QDs alter platelet function is a vital step in deciding if this nanoparticle can have biomedical applications as an imaging agent. With this in mind, a pipeline for investigating InP/ZnS QD-based platelet imaging probes has been created, as shown in **Figure 1**.

The InP/ZnS (core/shell) QDs are initially synthesized in organic media following a hot-injection protocol, followed by a phase transfer to aqueous media using different phase transfer agents (Figure 1). The fluorescent probes are then characterized using several optical techniques and their platelet biocompatibility is assessed via individually designed biological assays (platelet aggregation, flow cytometry, platelet spreading, and in vitro flow). Subsequently, this allows us to evaluate their potential application to imaging platelets.

Within this paper, we demonstrate that InP/ZnS QD interaction and activation of platelets are dependent on both the ligand used for phase transfer (TGA, Pen, LA, and GSH) and QD concentration in solution. Therefore, these properties of the QDs are critical for both imaging and biocompatibility with platelets and should be carefully selected before adding other components like platelet-specific conjugates, other imaging modalities, and drug therapies in the future.

2. Results and Discussion

2.1. Synthesis and Characterization of InP/ZnS QDs in Hexane

InP/ZnS core/shell QDs were synthesized via a hot-injection methodology in organic media.[6,15] Different indium precursors are used to tune the emission wavelength of these QDs. Previously, it was shown that higher atomic number halides yield smaller QD and therefore blueshifts their emission wavelength, which was attributed to the differences in reactivity of each halide.[15] In this work, the primary focus was $InCl_3$ as the indium halide, which resulted in the production of QDs that are larger (compared to those produced using InI_3 and $InBr_3$) and emit in the red region of the visible spectrum (620–750 nm). These results agree with the observations made by Tessier and co-workers.[15]

The optical properties of InP/ZnS QDs in hexane were measured using absorbance, emission, lifetime, and physical methodologies, shown below (**Figure 2**), prior to phase transfer and surface functionalization of the nanomaterial.

After the growth of the ZnS shell, absorbance measurements show an excitonic peak at 592 nm, while an emission maximum was observed at 627 nm with a full width at half maximum (FWHM) of 63 nm (Figure 2A). The average fluorescence lifetime shows a value of 39.6 ± 0.23 ns (**Table 1**). These values are consistent with the fluorescent properties previously reported for this nanomaterial.[6,15]

Transmission electron microscopy (TEM) images show quasispheroidal QDs (Figure 2) with an average diameter of 4.7 ± 1.3 nm, with an In:Zn ratio of 0.64:1.00 and In:P ratio of 0.42:1.00 (Table S1, Supporting Information) according to energy dispersive X-ray (EDX) spectroscopy (Figure 2F). Through these measurements it is possible to observe atomically resolved individual QDs and although the core structure cannot be identified, analysis of the line profiles in Figure 2E–H shows an average

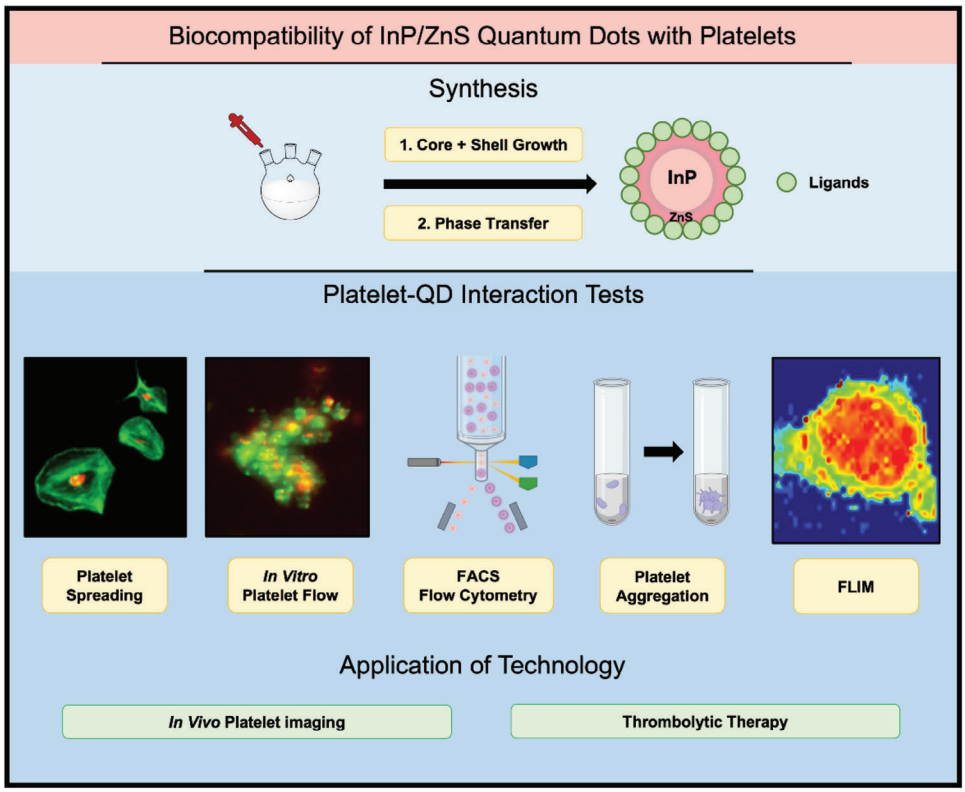

Figure 1. Schematic diagram showing the pipeline for a platelet-compatible imaging probe, which will first involve the synthesis of InP/ZnS QDs followed by surface functionalization, and then in vitro platelet biocompatibility testing.

lattice plane spacing of 3.27 Å, which is consistent with the cubic zinc blende phases of ZnS in the shell.[27]

2.2. Photophysical Characterisation of Water Dispersible InP/ZnS QDs

For use in a biological setting, QDs must be water-dispersible. However, as-synthesized QDs are hydrophobic. Therefore, InP/ZnS QDs were phase transferred into water with a series of hydrophilic capping ligands; thioglycolic acid (TGA), penicillamine (Pen), lipoic acid (LA), and glutathione (GSH). The photophysical characterization of these QDs is shown in **Figure 3**.

After phase transfer, absorbance measurements show an excitonic peak at 572–580 nm, and emission maxima for all InP/ZnS QDs capped with the different ligands were consistent at 617–622 nm with a FWHM of 59–66 nm (Figure 3A; Table S2, Supporting Information). The evident blueshift in emission is expected due to the etching of the surface atoms during the phase transfer protocol.

The average lifetime decay changes for InP/ZnS@TGA in water, with a value of 10.3 ± 0.06 ns (Table 1).[6] The lifetime in water is shorter than in hexane and includes an additional fast component (2.0 ± 0.03 ns) which could be indicative of decay pathways via vibrational energy levels of water or additional surface defects. These values are consistent with the fluorescent properties previously reported for this nanomaterial.[6]

TEM and distribution analysis of InP/ZnS@TGA gives a diameter of 5.4 ± 2.0 nm for the QDs. No difference in size can be observed following phase transfer through these TEM measurements due to the relatively large errors resulting from the low sampling density, however, these results confirm no significant morphological changes following phase transfer. EDX spectroscopy gives an In:Zn ratio of 0.87:1.00 and an In:P ratio of 1.03:1.00 (Table S1, Supporting Information). As previously seen, analysis of the line profiles in Figure 3E,F reveals an average lattice plane spacing of 3.1 Å, which is consistent with the cubic zinc blende phases of ZnS in the shell. The increase of In:Zn ratio (from 0.64:1.00) suggests an expected decrease in the Zn content from the surface, as some of these atoms are stripped away during phase transfer. The P content also decreases when compared to hexane QDs (In:P ratio of 0.42:1.00) potentially due to the loss of trioctylphosphine from the nanoparticle surface. The size distribution analysis supports a greater polydispersity in water, this occurs with all the phase transfer agents with LA showing the greatest polydispersity (Figure 3; Figure S1, Supporting Information). The choice of phase transfer ligand is important to maintain monodispersity and therefore the ideal optical properties. The additional characterization for GSH and Pen ligands can be found in Figure S2 (Supporting Information).

This apparent stripping of shell (Zn) materials could be related to the weaker photophysical properties of InP/ZnS QDs in water. Although the emission maxima do not significantly change in hexane and in water (≈627 nm), the photoluminescent

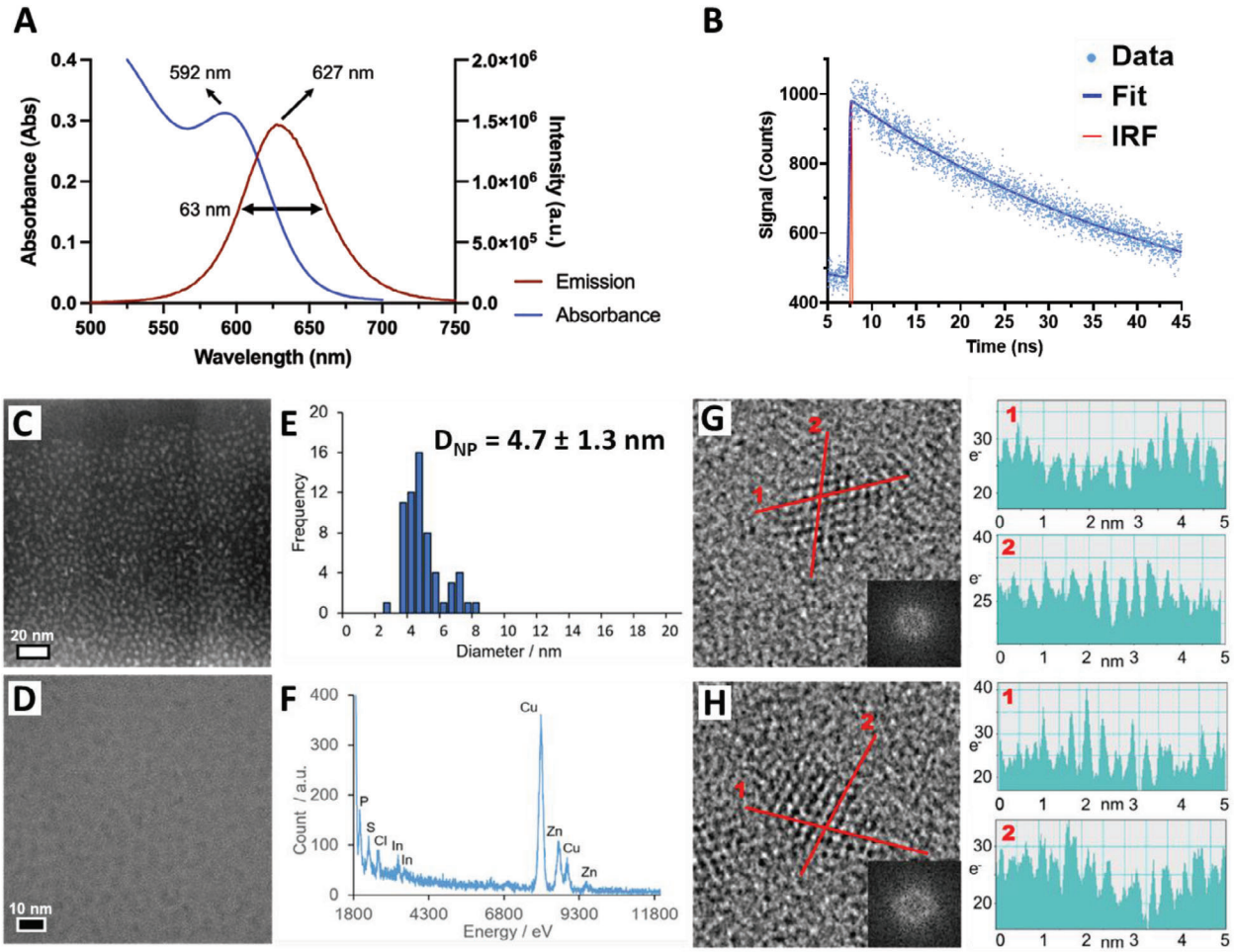

Figure 2. Photophysical properties of InP/ZnS QDs in hexane A) absorption (blue) and emission spectra (red) of red InP/ZnS QDs (using $InCl_3$ as a precursor) with indication of full width at half maximum and peak values. B) Normalised fluorescence decay curve of InP/ZnS in hexane (1 μM). C) Scanning transmission electron microscopy (STEM) image, D) high- resolution transmission electron microscopy (HRTEM image), E) size distributions were obtained by measuring 100–150 individual NPs, F) EDX spectrum (N.B. Cu peaks due to TEM grid), G,H) transmission electron microscopy (TEM) images of individual QDs (with fast Fourier transforms (FFT) inset) and corresponding line profiles. White and black scale bars are 20 and 10 nm, respectively. Spectra measured at 20 °C with excitation wavelength at 405 nm.

quantum yield (PLQY) changes drastically (Table S2, Supporting Information). The PLQY in hexane was measured at 44%, while in water there is a reduction of 35–61% when measuring the PLQY of GSH and TGA capped QDs, respectively. These results suggest that the phase transfer protocol is introducing defect sites on the surface of the QDs, by stripping away Zn atoms, which in turn creates additional electron traps that decrease the fluorescence efficiency of these nanomaterials. These differences could be enough to induce different biological responses when testing these nanoparticles in platelets.

Table 1. Analysis of the time-resolved measurements of red InP/ZnS QDs in different solvents.

QDs	Concentration [μM]	Average Lifetime [ns] [a]	χ^2	Decay Component [ns]	
				1 [b]	2 [b]
InP/ZnS (hexane)	1	39.6 ± 0.23	1.08	39.6 ± 0.23 (100%)	–
InP/ZnS@TGA (water)	1	10.3 ± 0.06	1.22	2.0 ± 0.03 (53.0%)	19.7 ± 0.13 (47.0%)

[a] The average lifetime refers to the amplitude average lifetime ($\tau_m = \sum_{i=1}^{n}(a_i\tau_i)$); [b] The uncertainty on individual lifetimes was determined using a variance-covariance matrix. The residuals for each fit can be seen in Figure S16 (Supporting Information).

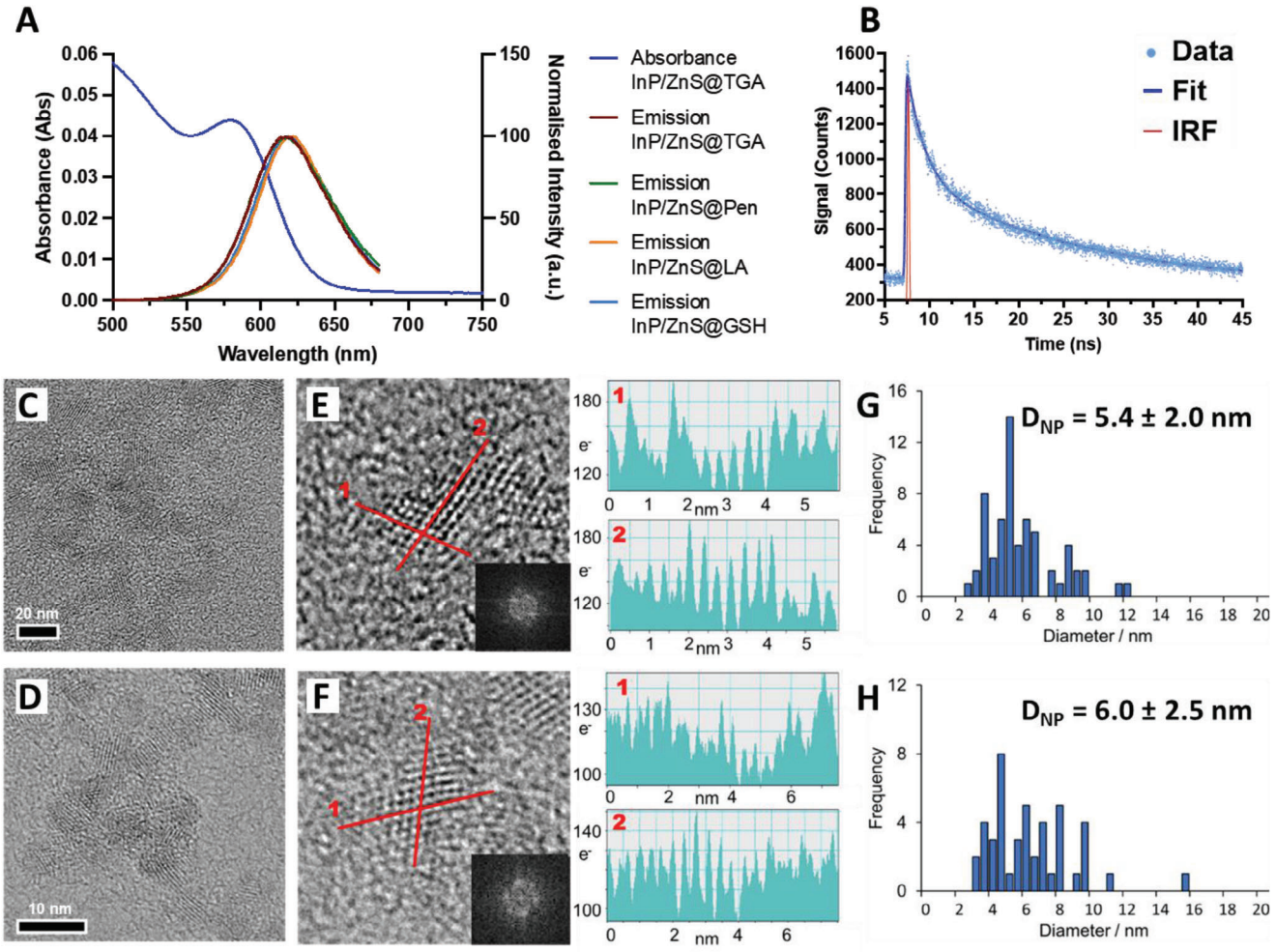

Figure 3. Photophysical properties of InP/ZnS QDs in water. A) Absorption and normalized emission spectra of red InP/ZnS QDs in water (using different phase transfer agents). B) Normalized fluorescence decay curve of InP/ZnS in water with TGA as the surface ligand (1 μM). C–H) Physical properties of Red InP/ZnS@TGA (middle row) and Red InP/ZnS@LA (bottom row) QDs. C,D) HRTEM images, E,F) TEM images of individual QDs (FFTs inset) and corresponding line profiles, and G,H) size distributions were obtained by measuring 100–150 individual NPs. Black scale bars are 10 nm. Spectra measured at 20 °C with excitation wavelength at 405 nm. All measurements were carried out in MilliQ water at 20 °C, pH 7.

2.3. Assessing InP/ZnS QD-Platelet Interactions in Washed Platelets

If InP/ZnS QDs are to be used biologically as the nanoparticle vehicle for imaging, it is vital to find the specific concentration that is compatible with platelets and shows no adverse effects. Careful consideration will be made to the potential effects that the ligands used to phase transfer the QDs may be having on the platelets.

Initially, we investigated if Pen, TGA, LA, and GSH induced platelet aggregation independent of natural platelet agonists. Analysis of the results shows that Pen, TGA, and GSH did not induce platelet aggregation. However, LA, at 100 μM and higher concentrations, induced significant platelet aggregation (Figure S4A,B, Supporting Information). In addition, we also investigated if these compounds affected the ability of natural platelet agonists, such as thrombin, to cause platelet aggregation. Therefore, we incubated washed platelets with varying concentrations of each of the ligands (100 nM–10 mM) for 10 min in stirring conditions before a high dose of agonist was added (0.1 U mL^{-1} thrombin) and monitored the aggregation. As shown in Figure S4C (Supporting Information), thrombin-induced aggregation was affected in LA samples that had already undergone aggregation to LA alone (100 μM and above). However, thrombin-induced platelet aggregation was unaffected by doses of 10 μM LA and below, and all concentrations of GSH and TGA were tested. Only Pen at high doses (1–10 mM) showed an inhibition of thrombin-mediated aggregation. Even though others have tested Pen, GSH, and LA in platelet aggregation, thrombin has not been used as the platelet agonist of choice in the washed platelets of healthy humans.[28–33] Although high concentrations of Pen and LA showed effects (either by preactivating platelets or affecting thrombin-mediated platelet aggregation), these concentrations are expected to be higher than the doses administered when using the highest QD concentration.

Therefore, as we could identify that the ligands at the appropriate concentrations had no effect on platelet function, we now checked to see what would happen to the platelet aggregation response if InP/ZnS QDs coated in these ligands were added to washed platelets. All InP/ZnS QD (**Figure 4**) permutations induced an aggregation response at concentrations of 100 nM, with varying degrees of significance. This response is measured by the change in light transmission through the sample in comparison to Tyrode's control, expressed as a percentage. InP/ZnS@TGA induced observably weaker aggregation (23.87 ± 5.33%, $p = 0.0354$) when compared to the other QDs; InP/ZnS@LA (84.23 ± 1.17%, $p<0.0001$), InP/ZnS@Pen (47.15 ± 7.82%, $p<0.0001$) and InP/ZnS@GSH (57.08 ± 7.21%, $p<0.0001$). This ligand-dependent aggregation response is also present at 30 and 10 nM, as the InP/ZnS@LA QDs still induce strong aggregation (30 nM–54.25 ± 6.76%, $p<0.0001$; 10 nM–20.87 ± 5.14%, $p = 0.0003$) whilst all other InP/ZnS QD-ligand permutations show little aggregation (Figure S5, Supporting Information). To confirm that the change in light transmission was due to platelet aggregation, and not QD-induced platelet agglutination, we used a platelet aggregation inhibitor eptifibatide. The eptifibatide successfully blocked the aggregation induced by 100 nM InP/ZnS@LA QDs. This indicates that QDs induced platelet aggregation via activation of integrin $\alpha_{IIb}\beta_3$ and not platelet agglutination (Figure S6, Supporting Information).

Importantly, we also checked platelet aggregation due to a natural platelet agonist, thrombin, post-QD incubation. The washed platelets were incubated with QDs for 10 min before being stimulated with a high dose of agonist (0.1 U mL^{-1} thrombin) and the response was monitored for a further 8 min (Figure S7, Supporting Information). From these results, there was a significant decrease in the aggregation response seen with thrombin when the washed platelets were preincubated with all QDs at 100 nM concentrations (InP/ZnS@LA, InP/ZnS@Pen and InP/ZnS@GSH; $p<0.0001$ and InP/ZnS@TGA; $p = 0.0152$). When decreasing the QD dose further to 30 nM, only the InP/ZnS@LA variant caused a hindered response to thrombin ($p = 0.0049$). When the platelets were incubated with all QDs at 10 nM concentrations, the response to thrombin was normal. This suggests that if QDs induce platelet aggregation independent of a natural ligand, platelet aggregation induced by agonists such as thrombin is reduced.

A further method of assessing platelet biocompatibility is by using static platelet binding assays. After an initial incubation of the QDs in washed platelets, platelets were then added to a coverslip coated with 100 μg mL^{-1} fibrinogen and left to spread for 25 min before fixation, staining, and imaging. These images can then identify both the number and the morphology of platelets that have adhered, and also the general QD localization. The emission of the QDs was shown to be compatible with the green FITC (fluorescein isothiocyanate) phalloidin actin stain used, as both channels gave distinct staining (Figure S8, Supporting Information). This method is particularly useful for the lower concentrations of QDs, as, although we have shown that platelet aggregation is not affected by most of the QDs at 10 nM, we do not know if the QDs and platelets were physically interacting in some other way. All the representative static platelet spreading images can be seen in Figure S9 (Supporting Information).

Figure S10 (Supporting Information) demonstrates that there was no significant difference in the number of platelets adhered, irrespective of the type and concentration of QDs used ($p = 0.3948$). In contrast, InP/ZnS@LA and InP/ZnS@GSH significantly decreased the size of the spread platelet (InP/ZnS@LA 12.68 ± 1.86 μm^2, $p<0.0001$; InP/ZnS@GSH 15.18 ± 2.85 μm^2, $p = 0.0010$) compared to the platelets not incubated with QDs (35.72 ± 2.24 μm^2) in a dose-responsive manner (Figure 4). This reduced surface area concurs with the aggregation data in that at 100 nM, both InP/ZnS@LA and InP/ZnS@GSH were able to activate the platelets to induce strong aggregation. This, therefore, suggests that activation was induced during the initial 20 min incubation and when the platelets were added to the fibrinogen matrix, the activated platelets were then unable to spread. Additionally, InP/ZnS@LA and InP/ZnS@GSH showed the greatest localization with the platelets, with InP/ZnS@LA localizing with 81.59 ± 10.73% of platelets and InP/ZnS@GSH localizing with 43.89 ± 6.96% of platelets at 10 nM concentrations ($p<0.0001$). Other permutations were shown to be less responsive, with InP/ZnS@Pen and InP/ZnS@TGA not affecting platelet spread size, even at 100 nM, and these types only significantly interacted with platelets at higher concentrations of 30 nM with InP/ZnS@Pen showing 41.34 ± 14.14% platelet localization and 14.49 ± 4.18% of platelets showing localization with InP/ZnS@TGA ($p<0.0001$ and $p = 0.0107$ respectively). When correlating this with the aggregation data, these two types of QD also only induced aggregation at high concentrations of 100 nM, so they are less reactive to the platelets when considering both the spreading and aggregation data.

To identify if the QDs bound to the platelet were within or outside the membrane of the platelet, z-stacks of the spread platelets were taken to form a 3D image. This analysis indicated that the QD fluorescent signal appears more on top of the platelet rather than within, implying that they may be binding to the surface rather than being taken up by the platelet (Figure S11, Supporting Information).

We also used flow cytometry to further identify the interaction of platelets with the QDs (Figure S12, Supporting Information). For the flow cytometry, platelets were stained using a platelet-specific CD41 antibody to identify them effectively within the solution. Both the % of platelets binding QDs and the fluorescent intensity of the QD signal emitted were observed for InP/ZnS@LA, InP/ZnS@Pen, and InP/ZnS@TGA. This data showed a similar trend to the static adhesion results whereby the InP/ZnS@LA showed the highest interaction with a high proportion of platelets emitting a QD signal at concentrations of 10 nM. On the other hand, InP/ZnS@TGA showed few QDs interacting with basal platelets, even at higher concentrations of 100 nM ($p = 0.9969$), suggesting that this permutation interacts the least. Interestingly although the number of platelets that bound the QDs was very different between TGA and LA QDs, the average mean fluorescence intensity (MFI) for the population of platelets positive for QDs, was not significantly different between the populations.

These studies in washed platelets suggest the best ligands for QDs when imaging platelets will be TGA and penicillamine as they have no effect on spreading and reduced effect on aggregation even at 100 nM. This range also marries nicely with the good optical properties of this QD variant, which makes this variant advantageous if used for imaging. However, when considering its application in imaging and therapeutics, it appears that

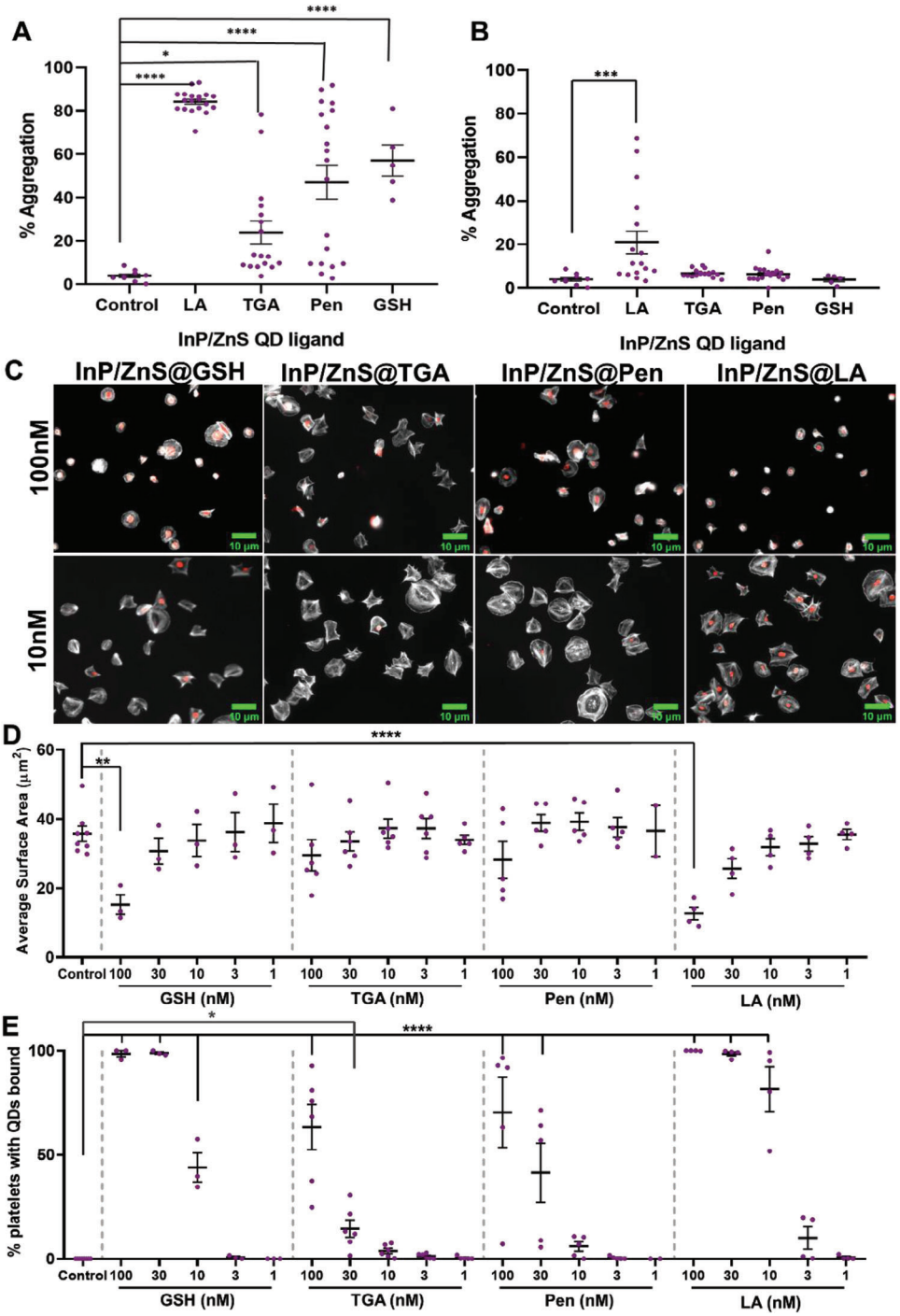

Figure 4. Washed platelet aggregation is induced by red InP/ZnS QD variants in a dose-dependent manner (A,B) and interaction with spread platelets with the InP/ZnS QDs appears to be ligand-dependent (C–E). For the platelet aggregation data, washed platelets at a concentration of 2.5×10^8 mL^{-1} were incubated at 37 °C for 10 min with either a blank control (Tyrode's buffer; pH 7.3) or a different ligand permutation of InP/ZnS QDs [either InP/ZnS@LA (n = 19), InP/ZnS@TGA (n = 17), InP/ZnS@Pen (n = 19) and InP/ZnS@GSH (n = 5)] at either 100 nM (A) or 10 nM (B). Statistical analysis (in the form of an Ordinary one-way ANOVA with a Tukey's multiple comparison post hoc test) was performed comparing the % aggregation of each permutation compared to the basal Tyrode's control. All QD types induced aggregation at 100 nM concentration whereas only InP/ZnS@LA was shown to induce significant aggregation at 10 nM. QD-platelet interaction was also seen at these concentrations during the spreading assay, with the representative images being shown in (C). For this spreading assay, platelets at a concentration of 2×10^7 mL^{-1} were incubated with varying concentrations of red InP/ZnS QDs for 20 min before being spread on 100 μg mL^{-1} fibrinogen for 25 min (TGA-n = 6, Pen-n = 5, LA-n = 4, GSH-n = 3). The samples were then fixed, permeabilized, and stained with FITC phalloidin for 45 min before being mounted onto glass slides and imaged using conventional microscopy. From the quantification carried out, only InP/ZnS@GSH and InP/ZnS@LA at concentrations of 100 nM significantly reduced the spread platelet size (D). InP/ZnS@TGA and InP/ZnS@Pen could be used at 10 nM without significant QD binding being observed (E). * Significant at p value <0.05, ** significant at p value <0.01; *** significant at p value <0.001; **** significant at p value <0.0001.

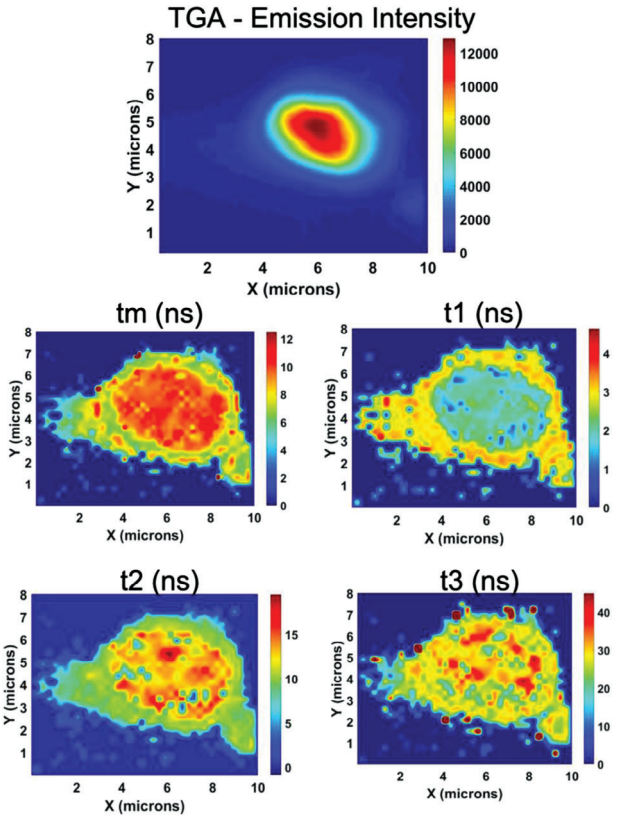

Figure 5. FLIM measurements of InP/ZnS@TGA QDs incubated with washed platelets. The images were acquired with an excitation wavelength of 405 nm and emission of 620 nm at 20 °C.

InP/ZnS@TGA and InP/ZnS@Pen can be used in the range of ≈10–30 nM without adverse effects on platelet functionality.

2.4. Fluorescence Lifetime Imaging Microscopy (FLIM)

To further confirm our findings of QD-platelet interaction and look at the fluorescent properties of QDs after platelet interaction in more depth, we used fluorescence lifetime imaging microscopy (FLIM). FLIM can give valuable information, such as fluorescent lifetimes, in addition to the information that is typically obtained by conventional microscopy. This will provide additional information about the interaction of platelets with QDs, beyond morphological changes. For the FLIM measurements, washed platelets were incubated with InP/ZnS QDs for 20 min and then allowed to spread on a coverslip coated in 100 μg mL^{-1} fibrinogen for a further 25 min. The samples were then fixed with 4% paraformaldehyde and mounted onto glass slides. After incubating platelets with InP/ZnS@TGA QDs, the lifetime of the sample was mapped, and the results are shown in **Figure 5**.

The intensity image shows a centralized QD population on the platelet, in agreement with the fluorescent microscopy data (**Figure 4**; Figure S11, Supporting Information). A multi-exponential decay model was used to fit the FLIM decay curve. Average lifetime measurements (τ_m) show QDs predominately localized toward the center of the platelet with smaller clusters distributed toward the edges, all with a value between 8–10 ns, a similar value found for the lifetime of the same QDs in water (Table 1). Mapping the first decay component (τ_1) shows a correspondingly shorter lifetime in the center of the platelet (1–2 ns) and longer toward the edge of the cell (3–4 ns). In parallel the τ_2 mapping reveals longer lifetime values (≈15 ns) in the center where QDs appear to be in higher concentration and lower values toward the edge (≈9 ns). These changes in τ_1 and τ_2 could be potentially linked to energy transfer within the QD population as a function of localization/concentration.[34–36] In this scenario, the decreased τ_1 corresponds to donor QDs transferring energy to acceptor QDs, and the increase in τ_2 reflects the additional time for energy transfer.[34–36] The same pattern of InP/ZnS lifetimes in the platelet can also be seen with other formulations such as InP/ZnS@Pen and InP/ZnS@LA (Figure S15, Supporting Information). Comparing these results to those previously obtained for InP/ZnS QDs in water, and of the fluorescence microscopy of platelets exposed to these QDs, we propose a similar mechanism is occurring; the QDs are localizing on and around the platelet resulting in areas with higher local concentrations. This leads to increased energy transfer from smaller to larger QDs in these regions due to the reduced inter-particle distance. When interacting with platelets, the spatial distribution within the platelet may cause the QDs to aggregate, leading to radiative energy transfer and self-quenching mechanisms. This could explain the measured values of the different lifetime components (τ_m, τ_1, and τ_2) in the FLIM experiments.

2.5. Assessing InP/ZnS QD-Platelet Interactions in Platelet-Rich Plasma and in Whole Blood

For the data identified within a washed platelet-based system to be truly applicable, it was important to test the QDs with platelets in a plasma suspension (platelet-rich plasma–PRP) and in whole blood to provide a better insight into how these QDs might interact with platelets in vivo. As shown in **Figure 6**, even at concentrations of 100 nM, there was no significant aggregation induced by InP/ZnS@LA ($p = 0.9420$), InP/ZnS@Pen ($p>0.9999$), or InP/ZnS@TGA ($p = 0.2861$). The presence of the QDs in the PRP also did not cause any significant changes in aggregation response to 3 μg mL^{-1} collagen, even with PRP incubated with 100 nM InP/ZnS@LA ($p = 0.9976$), InP/ZnS@Pen ($p = 0.9992$) or InP/ZnS@TGA ($p = 0.5623$). This therefore suggests that some property of the plasma is preventing the induction of platelet aggregation by the QDs. This may be due to a component of the plasma binding to the surface of the QDs. The average association constant, K_A, between InP/ZnS@TGA and bovine serum albumin (BSA) was found to be 3.97×10^6 M^{-1} (Figure S13, Supporting Information). This however does not necessarily correlate to the QDs not interacting with the platelets at all in the presence of plasma proteins. To identify if there was any platelet interaction in the presence of plasma proteins, whole blood was incubated with QDs at 10 nM before flowing it through a microfluidic chip precoated with 100 μg mL^{-1} collagen for 4 min to form platelet-rich thrombi. Analysis of the fixed thrombi via confocal microscopy identified that all types of QDs were enveloped within the formed thrombi (Figure S14, Supporting Information). This therefore suggests that when adding the QDs to plasma, the

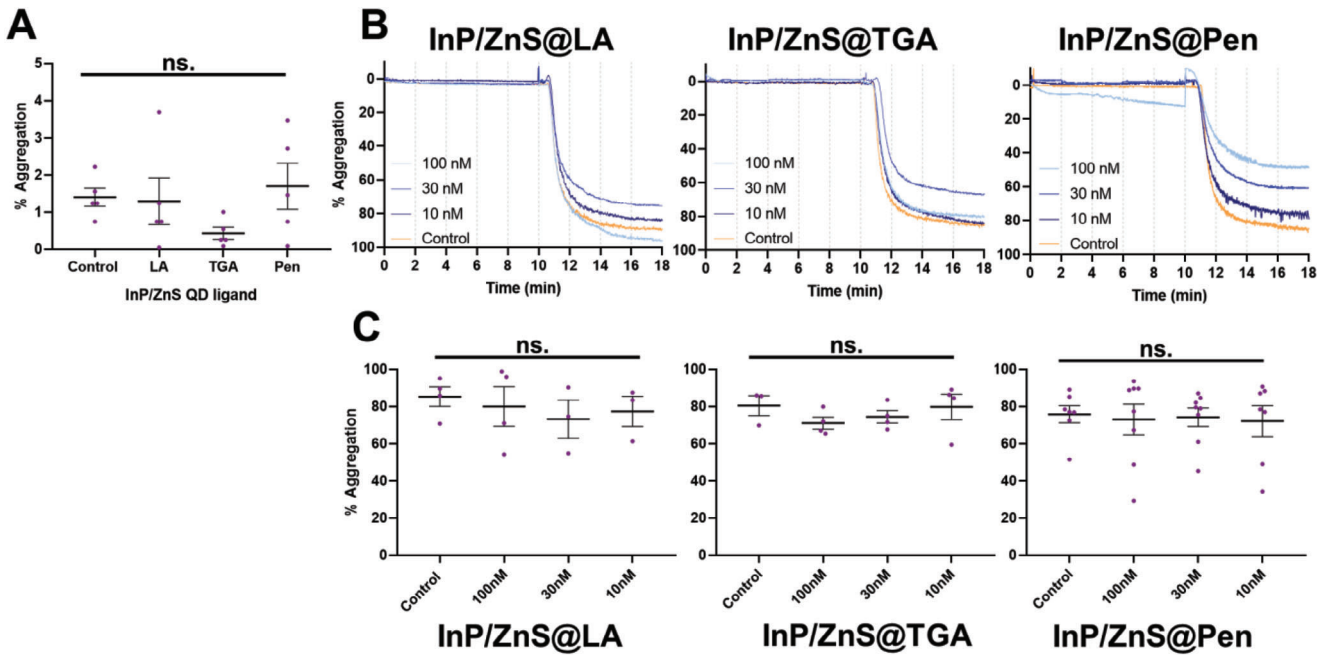

Figure 6. The presence of up to 100 nM of each QD did not induce any significant change to the aggregation response (A) and this is seen both with and without agonist within the representative traces (n=5) (B) and with the comparative analysis post collagen injection (C). Platelet-rich plasma was incubated at 37 °C with varying concentrations of either InP/ZnS@LA ($n = 4$), InP/ZnS@TGA ($n = 4$), InP/ZnS@Pen ($n = 8$) or PBS (as non-QD control) for 10 min before 3 μg mL^{-1} collagen was added and the response monitored for a further 8 min. Statistical analysis (in the form of an Ordinary one-way ANOVA with a Tukey's multiple comparison post hoc test) was performed comparing the % aggregation of each permutation compared to the basal PBS control. From the statistical analysis carried out, there was no significant aggregation response induced by any QD type at 100 nM concentration ($p = 0.2383$) nor was there any significant change in aggregation to 3 μg mL^{-1} collagen in the presence of InP/ZnS@LA ($p = 0.7933$), InP/ZnS@TGA ($p = 0.4498$) or InP/ZnS@Pen ($p = 0.9946$). The ns. notation denotes non-significance, whereby $p>0.05$.

associated reactivity of QDs with platelets is removed, but the QDs are still able to be enveloped within the thrombi.

3. Conclusion

InP/ZnS QDs have received a larger focus in recent years as a safer alternative to heavy metal-based QDs in biological applications. Although the focus has been on improving the photophysical properties in water with various ligands, little is known about how these QDs impact the biological function of the platelet and their photophysical behavior within the platelet. We have synthesized and characterized InP/ZnS QDs in hexanes and phase-transferred them to aqueous media using different phase transfer agents such as thioglycolic acid (TGA), penicillamine (Pen), lipoic acid (LA) and glutathione (GSH). When testing the ability of InP/ZnS QDs to interact with platelets, we have shown that this interaction is dependent on the ligand used for phase transfer and the concentration of QDs in solution. Platelet aggregation assays have shown that all of the tested QD permutations can induce platelet aggregation at concentrations of 100 nM and this becomes significantly weaker below 30 nM, except for InP/ZnS@LA QDs which still displayed high aggregation at 10 nM. Static adhesion assays confirmed that high concentrations of InP/ZnS@LA and InP/ZnS@GSH interact with platelets and induce morphology changes, while InP/ZnS@TGA and InP/ZnS@Pen had no effect on platelet spreading, even at 100 nM. Using confocal microscopy, and FLIM, it has been shown that InP/ZnS QDs with all these ligands remain on the surface of platelets localizing in high concentration toward the center of the cell. The FLIM measurements show a potential energy transfer within this high QD localization/concentration.

In summary, biological studies on platelets have highlighted that both TGA and Pen-capped QDs appear to be the most platelet biocompatible permutation tested. These types can be used at concentrations ranging from 10–30 nM in washed platelets and up to 100 nM in platelet-rich plasma without any detrimental impact on platelet aggregation or spread platelet morphology whilst still retaining good fluorescent properties. These results are thus an important stepping point for the development of fluorescent probes for platelet imaging.

4. Experimental Section

General Procedures: All chemicals used in this work were purchased from Sigma Aldrich (Dorset, UK) and solvents were purchased from VWR (Leicestershire, UK) unless stated otherwise. Indium chloride (99.999%), indium iodide (99.999%), indium bromide (99.999%) and zinc chloride (99.999%), tris(diethylamino)phosphine (97%), sulfur powder (90%), D-penicillamine (90%), L-glutathione reduced (98%), (±)-α-lipoic acid (98%), trioctylphosphine (90%), tetramethylammonium hydroxide solution (25 wt.% in H_2O), 1-octadecene (technical grade, 90%), oleylamine (technical grade, 70%). All products were used without further purification. Water (H_2O) was purified before each use with a Millipore Milli-Q system, with a resistivity value of 18 MΩ cm corrected at 25 °C.

High-resistance, single-use syringes (Injekt Luer Solo) and needles used in this work were purchased from Braun Medical Ltd.

Reactions including oxygen or moisture-sensitive compounds were carried out under a dry N_2 or Ar atmosphere. The used glassware was dried in a 150 °C oven and cooled under argon pressure immediately before use, with the use of a Schlenk line. Standard syringe and septa techniques were employed.

Reactions at high temperatures were conducted using IKA C-MAG HS7 hotplate stirrers with temperature regulators together with heating blocks for better heating efficiency. Auxiliary thermometers were used to confirm the internal temperature of the solutions. Reaction temperatures refer to internal solution temperatures unless stated otherwise.

UV–Vis absorption spectra for the characterization of QDs were recorded on a PerkinElmer Lambda 365 UV–vis using 2 × 10 mm cuvettes. Fluorescence measurements were performed using an Edinburgh Instruments FS5 spectrofluorometer, in 2 × 10 mm quartz cuvettes, using a front-facing holder. Lifetime measurements have been analyzed using a variance-covariance matrix method for 1, 2, and 3 exponential decays to refine fits and determine the uncertainty of each decay component. The uncertainty of the amplitude average lifetime was calculated using standard error propagation from the uncertainty of the individual lifetimes.

Hydrodynamic diameter and Zeta potential of QDs in solution were measured on a Malvern Panalytical Zetasizer Nano ZS. Plastic cuvettes (10 mm) were used for both measurements and a universal "dip" cell was additionally used for Zeta potential measurements.

TEM was undertaken on a FEI Titan3 Themis G2 operating at 300 kV fitted with 4 EDX silicon drift detectors and a Gatan One-View CCD. Bruker Esprit software (Version 1.9.4) was used for EDX spectra collection and analysis. High-angle annular dark field scanning TEM (STEM) and EDX mapping were conducted using a probe current of ≈150 pA. Samples were prepared for TEM by placing a drop of suspended QDs on a graphene oxide-coated holey carbon film supported on a copper TEM grid (EM Resolutions, UK). QD sizing was performed by measuring the diameter of ≈100–150 individual QDs per sample) in the STEM images.

Preparation of Shell Precursor's Reactions: Preparation of TOP-S 2.2 M (sulfur precursor): Sulfur (353 mg, 22 mmol) in trioctylphosphine (10 mL, 22 mmol, TOP) was stirred and degassed at 120 °C for 1 h with alternating vacuum and argon cycles. The final solution was left under an inert atmosphere of argon, stirring at 120 °C.

Preparation of zinc stearate 0.4 M in 1-octadecene (zinc precursor): zinc stearate (5000 mg, 8.0 mmol) in 1-octadecene (20 mL, 62.5 mmol) was stirred and degassed at 150 °C for 1 h with alternating vacuum and argon cycles. The final solution was left under an inert atmosphere of argon, stirring at 150 °C.

Synthesis of InP Core Quantum Dots: The synthetic methodology for the preparation of size-tuneable QDs were adapted from the work described by Clarke and co-workers and Tessier and co-workers.[6,15]

Indium(III) chloride, bromide, or iodide (0.45 mmol) and zinc(II) chloride (300 mg, 2.2 mmol) in oleylamine (5.0 mL, 15 mmol) were stirred and degassed, with alternating cycles of Ar and vacuum, at 120 °C for an hour and then heated to 190 °C under inert atmosphere. Upon reaching and stabilizing at 190 °C, tris-(diethylamino)phosphine (0.45 mL, 1.6 mmol, phosphorus:indium ratio = 3.6:1) was quickly injected into the above mixture. The core growth took place for 20–30 min, depending on the indium precursor used (20 min for InI_3, 30 min for $InCl_3$ and $InBr_3$).

TOP-S (1 mL, 2.2 M) was added by slow injection. The solution was stirred at 180 °C for 40 min. The temperature was rapidly increased to 200 °C and stirring continued for 1 h. Zinc stearate (4 mL, 0.4 M in 1-octadecene) was added by slow injection. The temperature was immediately rapidly increased to 220 °C and the solution was stirred for 30 min. TOP-S (0.7 mL, 2.2 M) was added by slow injection. The reaction temperature was immediately increased to 240 °C and stirred for 30 min. Zinc stearate (2 mL, 0.4 M in 1-octadecene) was added by slow injection. The temperature was immediately rapidly increased to 260 °C and stirred for another 30 min. The reaction was cooled to 180 °C. After stabilizing at that temperature for 30 min, the synthesis of the second shell began with an injection of TOP-S (1 mL, 2.2 M), repeating the process of the first shell. After the last zinc stearate injection, the reaction was then cooled to room temperature. Chloroform (5 mL) was added to the mixture, and it was then poured into a 50 mL falcon tube filled with 20 mL ethanol. The QDs were then centrifuged at 3400 rpm for 6 min, the supernatant discarded, and the pellet resuspended in hexane. The QDs were stored at a low temperature (4 °C) for further characterization.

Phase Transfer and Surface Functionalization of InP/ZnS QDs: Phase transfer of InP/ZnS QDs from organic to aqueous phase was accomplished following a procedure reported by Tamang and co-workers.[17] Initially, 1 mL of QDs stored in hexane were centrifuged (3 000 rpm, 1 min) to precipitate any residue of stearate suspended in solution. A thorough purification was conducted to remove additional hydrophobic molecules. Anhydrous ethanol (3 mL) was added and the suspension was centrifuged (10 000 rpm, 6 min). The supernatant was discarded, and the QDs were resuspended in chloroform (1 mL). Ethanol (3 mL) was added and the mixture was centrifuged (10 000 rpm, 6 min). The supernatant was discarded and the QDs were resuspended in a minimum amount of chloroform (1 mL). In a glass vial, the previously prepared InP/ZnS QDs in chloroform (1 mL) and a solution of the desired ligand (2 mL, 0.2 M) in degassed milli-Q water (18 MΩ) were mixed. Tris(2-carboxyethyl)phosphine hydrochloride (TCEP, 0.5 M, 250 µL) was added to the mixture and the pH was adjusted to 10 (TGA, GSH), 11 (penicillamine) or 12 (LA) by dropwise addition of 0.5 M tetramethylammonium hydroxide. LA was reduced in situ by TCEP during this process. The mixture was vigorously stirred at room temperature for 1 h, shielded from direct light. QDs in the aqueous phase were distributed into VWR centrifugal filters (30 kDa for red QDs, 10 kDa for green and orange QDs) at 6 000 rpm for 2 min. Then, 200 µL of milli-Q water was used to wash the QDs, and centrifugation was repeated. QDs were washed until the pH of the solution reached seven and the sample was then stored in the dark at 4 °C for further characterization.

Preparation of Washed Platelets from Healthy Human Blood: Whole blood from healthy human participants was obtained in Acid Citric Dextrose (ACD) vacutainers (BD). The blood was centrifuged twice, once at 700 rpm and then again at 900 rpm for 10 min per spin and the plasma was collected after each spin. Citric acid (0.3 M) was added to the PRP before being centrifuged again at 1000 × g for 10 min. The suspension was removed, and the pellet was resuspended in platelet wash buffer [0.036 M citric acid; 0.010 M EDTA; 0.005 M glucose; 0.005 M potassium chloride; 0.09 M sodium chloride]: with ≈1 mL of wash buffer being added per 10 mL of whole blood taken and the suspension was centrifuged at 1000xg for 10 min. The suspension was then removed, and the pellet resuspended in 1 mL of Tyrode's buffer [20 mM HEPES; 134 mM sodium chloride; 2 mM potassium chloride; 0.34 mM sodium hydrogen phosphate; 5.6 mM D-glucose anhydrase; 12 mM sodium hydrogen carbonate; 1 mM magnesium chloride]. The platelet count of the washed platelets was then measured using a Beckman Z1 colter particle counter and adjusted to a concentration of 2.5×10^8 platelets mL^{-1} using Tyrode's buffer.

Performing Light Transmission Aggregations (LTA) with the InP/ZnS QDs: All light transmission aggregations (LTA) were carried out using optical aggregometers Chronolog Model 490 4+4 (Chronolog, USA) alongside the provided AGGRO/LINK8 software (Chronolog, USA). The agonists used for the LTA include thrombin at 0.1 U mL^{-1} (Sigma-Aldrich, Dorset, UK) and collagen Reagens HORM Suspension (Takeda, Linz, Austria) at 3 µg mL^{-1}. For the washed platelet aggregations, washed platelets at a concentration of 2.5×10^8 platelets mL^{-1} were incubated with the QDs at 37 °C (at concentrations of 10–100 nM) for 10 min, and for this Tyrode's was used as the blank control. For the ligand aggregations, ligands at varying concentrations (100 nM–10 mM) were incubated for the same duration as the QD aggregations before being stimulated and left for a further 10 min with 0.1 U mL^{-1} thrombin. For the Eptifibatide studies, washed platelets were incubated with 9 µM Eptifibatide (TOCRIS, Bristol, UK) for 2 min before either the QD or the thrombin was added and left for 10 min. The QD dose-response curve produced with the AGGRO/LINK8 software was exported to Microsoft Excel and graphed and analyzed using GraphPad Prism 8.0 software (GraphPad, California, USA). The aggregation values were extrapolated 8 min post-QD/ligand injection and 8 min post thrombin injection. The data was then analyzed statistically for significance.

Performing Platelet Spreading Assays with the InP/ZnS QDs: Coverslips were placed into a 24-well plate and were coated with either 200 µl of 100 µg mL^{-1} fibrinogen or with 30 µl of 100 µg mL^{-1} collagen: these were left at room temperature for 1 h. During this incubation period, 5 mg mL^{-1} bovine serum albumin (BSA) was prepared by first dissolving in PBS, boiling for 10 min, and filtering through a 0.45 µm filter. After the 1 h incubation with the agonists, the wells were washed twice with PBS to remove any unbound agonist, and 300 µl BSA was added to each coverslip and left for 1 h at room temperature to prevent any non-specific binding of the platelets to the glass coverslip before being washed again twice with PBS. Human-washed platelets were prepared at a concentration of 2×10^7 platelets mL^{-1} and after the BSA had been washed off, 200 µl of washed platelets were added to each coverslip with varying concentrations of InP/ZnS QDs (10, 30, and 100 nM) as a 1:100 dilution and these were left to spread for 25 min at 37 °C. After 25 min, the coverslips were again washed twice with PBS. The slides were then fixed for 10 min with 4% paraformaldehyde, permeabilized with 0.1% Triton X-100 for 5 min, and stained with 2 mM FITC-phalloidin for 1 h at room temperature in the absence of light (washing twice with PBS in between each of these steps). The coverslips were then washed twice with PBS and mounted onto a glass slide using a drop of Diamond Antifade Mountant. The slides were then imaged on a Zeiss Axio Imager fluorescence microscope using an x63 oil immersion objective (1.4 NA). Images were taken using the Zen Pro software (Zeiss, UK). Parameters such as platelet adherence, surface area, and observable platelet-QD binding were identified using ImageJ (NIH, Bethesda, USA).

Performing FLIM Measurements of InP/ZnS QDs on Spread Washed Platelets: Coverslips were initially coated with 100 µg mL^{-1} fibrinogen for 1 h at room temperature before being washed twice with PBS and then blocked using 5 mg mL^{-1} BSA for an hour. Washed platelets prepared at concentrations of 2×10^7 platelets mL^{-1} were preincubated for 20 min at 37 °C with varying QD types and concentrations before being added to the coverslip after washing out the BSA. The washed platelet and QD suspension were left to spread on the fibrinogen-coated coverslip at 37 °C for 25 min. After which, the coverslips were washed twice and fixed using 4% paraformaldehyde at room temperature for 10 min. The coverslips were then mounted onto a glass slide using a drop of Diamond Antifade Mountant and then used for fluorescent-lifetime imaging microscopy.

Time-resolved fluorescence measurements were recorded using a home-built optical microscope. For FLIM measurements, the sample was scanned using a Nano-LPS 100 piezo-stage in a reflection configuration. A pulsed 405 nm laser diode was used to excite the photoluminescence using a 100× magnification Olympus objective with numerical aperture NA = 0.9. The same objective was used to collect the emission, which was then directed toward a microHR Horiba spectrometer and dispersed using a 150 line mm^{-1} grating onto an HPM-100 time-correlated single-photon counter. The setup had a temporal resolution of 0.1 ns. The integration time per pixel was defined by the level of photoluminescence, which, along with the selected spatial resolution, determined the scan duration. A pixel acquisition time of 1.5 s and a lateral step of 250 nm resulted in the total duration of each scan of 35–40 min (≈1200–1600 pixels per scan). The decay curves for each point were analyzed using the SPC Image software (Becker & Hickl). The average lifetime reported was calculated using:

$$\tau_{ave} = \sum_{i=1}^{n} \alpha_i \tau_i \quad (1)$$

where τ_i are the decay times, α_i the amplitudes of the decay components at $t = 0$, and n is the number of decay times.[37]

Performing Platelet in vitro Flow Assays with the InP/ZnS QDs: For the in vitro flow assays, microfluidic biochips (Vena8 Endothelial+ Microfluid Biochips, Cellix: Dublin, Ireland) were precoated overnight with 100 µg mL^{-1} collagen at 4 °C. On the following day, 5 mg mL^{-1} BSA was added and left for 15 min at room temperature to prevent the platelets from binding elsewhere in the biochip capillary. Healthy human blood was collected in 40 µM PPACK and then stained using a membrane stain (10 µM DIOC6 also known as 3,3'-Dihexyloxacarbocyanine iodide) prior to all flow experiments. Varying concentrations of InP/ZnS QDs (10, 30, 100 nM) were added to the stained whole blood and left in an Eppendorf for 20 min. After the 20 min incubation, the blood and QD suspension flowed over the chip at arterial shear 1000 m s^{-1} for 4 min to allow the thrombi to build up. After the 4 min, PBS then flowed over the chip to wash out any remaining red blood cells. The thrombi were then fixed with 4% paraformaldehyde and imaged using an Apetome.2 confocal units on a Zeiss Axio Observer using the Zeiss Zen software (Zeiss, UK). Z stack images were then taken using an x63 oil immersion objective (1.4 NA) and then concatenated into a video using ImageJ software (NIH, Bethesda, USA).

Performing Flow Cytometry with the InP/ZnS QDs: Washed platelets were diluted to 1×10^7 $platelets^{-1}mL$ in modified Tyrode's buffer and were incubated for 20 min in the dark at room temperature with varying concentrations of QDs (100–10 nM). Platelets alone were stained with a platelet-specific CD41 FITC antibody (BioLegend, California, USA). Unstained samples were also processed. Platelets were fixed by the final concentration of 0.45% cold PFA and immediately analyzed. BD LSR Fortessa cell analyzer (BD Bioscience, New Jersey, USA) was used to acquire events. Samples were analyzed using the same configuration baseline validated each experimental day with CS&T procedures. For each condition, 10 000 events were read from each sample by the FACSDiva Software (BD Biosciences, New Jersey, USA) and were then analyzed.

Fluorometric Assessment of QD-Bovine Serum Albumin (BSA) Interaction: Emission spectra ($\lambda_{ex} = 280$ nm) of samples containing BSA (5 µM) in PBS and increasing quantities of either InP/ZnS@TGA (0–0.3 µM) or InP/ZnS@LA (0–0.35 µM) were collected. The emission maxima of BSA ($\lambda_{em} = 350$ nm) were used to perform a Stern-Volmer analysis to determine association constants, K_A, of the QDs with BSA based on fluorescence quenching. Data was fit using non-linear regression in GraphPad 9.5.1.[38]

Statistical Analysis: Data has been reported to a maximum of two decimal places as averages and variation between averages (M±SEM). N numbers for the individual experiments were stated within the figure legends. Statistical analysis for the biological studies was carried out using Prism 8.0 software (GraphPad, California, USA). For the platelet aggregation analysis, to transform the raw exported data from the AGGRO/LINK8 software into percentage platelet aggregation, the data was first transformed by $y = 100\text{-}y$ and then normalized by defining the range of the data points of 0% as $y = -13$ and 100% as $y = 87$. Any percentage values obtained during the platelet studies were first Arcsine transformed ($y = \arcsin(\mathrm{sqrt}(y/100))$) to a numerical value instead of a percentage to meet the requirements for a one-way ANOVA. From there, a one-way ANOVA was performed to determine the significance between the different QDs. Further statistical testing was carried out post hoc with Turkey's multiple comparison test once a normality test was passed and the data was shown to be normally distributed. P values greater than or equal to 0.05 were considered significant.

Donor Recruitment: For the biological studies, written informed consent was acquired prior to the donation of blood. The blood was collected from healthy drug-free volunteers in accordance with Hull York Medical School Ethics Committee for "The study of platelet activation, signaling, and metabolism" and NHS REC study "Investigation of Blood cells for research into Cardiovascular Disease" (21/SC/0215).

Supporting Information

Supporting Information is available from the Wiley Online Library or from the author.

Acknowledgements

The authors would like to thank GJS and SDJC for their academic support and guidance throughout this work. This work was carried out with the financial support of the Medical Research Council (MR/T002573/1 for GJS, LNA, and TWP) and University of Hull PhD fellowships (HMG, ZB). The authors would also like to acknowledge the previous work done by MA on

InP/ZnS QDs which helped to guide this work and therefore their previous funding from the British Heart Foundation (FS/16/62/32220).

Conflict of Interest

All authors declare no conflict of interest.

Author Contributions

H.M.G. and Z.B. contributed equally to this work. H.M.G., T.W.P., and G.J.S. designed the chemistry-based QD experiments. H.M.G., T.W.P., and J.L. carried out the QD synthesis. T.W.C. conducted the TEM measurements. A.M., A.M.A., and J.-S.G.B. carried out the QD fluorescent lifetime measurements. Z.B. and S.D.J.C. designed the biological platelet studies. Z.B. carried out the platelet aggregation, spreading, and flow assays. Z.B. carried out all biological-based data analysis. L.N.-A. carried out the flow cytometry. M.A. conducted previous QD synthesis and biological studies which helped to guide this research. H.M.G., Z.B., G.J.S., and S.D.J.C. drafted the manuscript, and all authors had edited it.

Data Availability Statement

The data that support the findings of this study are available in the supplementary material of this article.

Keywords

fluorescence lifetime imaging microscopy (FLIM), fluorescence, hot-injections, InP/ZnS quantum dots (QDs), platelet imaging, platelets biocompatibility

Received: June 9, 2023
Revised: October 24, 2023
Published online: November 9, 2023

[1] M. L. Alonso-Alonso, M. Pérez-Mato, A. Sampedro-Viana, C. Correa-Paz, P. Ávila-Gómez, T. Sobrino, F. Campos, J. Castillo, R. Iglesias-Rey, P. Hervella, *Pharmaceutics* **2022**, *14*, 2156.
[2] V. Karagkiozaki, S. Logothetidis, N. Kalfagiannis, S. Lousinian, G. Giannoglou, *Nanomed.: Nanotechnol. Biol. Med.* **2009**, *5*, 64.
[3] D. Vasudevan, R. R. Gaddam, A. Trinchi, I. Cole, *J. Alloys Compd.* **2015**, *636*, 395.
[4] P. Reiss, M. Carriere, C. Lincheneau, L. Vaure, S. Tamang, *Chem. Rev.* **2016**, *116*, 10731.
[5] T. Jamieson, R. Bakhshi, D. Petrova, R. Pocock, M. Imani, A. M. Seifalian, *Biomater* **2007**, *28*, 4717.
[6] M. T. Clarke, F. N. Viscomi, T. W. Chamberlain, N. Hondow, A. M. Adawi, J. Sturge, S. C. Erwin, J.-S. G. Bouillard, S. Tamang, G. J. Stasiuk, *Commun Chem* **2019**, *2*, 36.
[7] Y.-H. Won, O. Cho, T. Kim, D.-Y. Chung, T. Kim, H. Chung, H. Jang, J. Lee, D. Kim, E. Jang, *Nature* **2019**, *575*, 634.
[8] B. Chen, D. Li, F. Wang, *Small* **2020**, *16*, 2002454.
[9] P. Samokhvalov, M. Artemyev, I. Nabiev, *Chem. - Eur. J.* **2013**, *19*, 1534.
[10] S. Hussain, N. Won, J. Nam, J. Bang, H. Chung, S. Kim, *ChemPhysChem* **2009**, *10*, 1466.
[11] V. Chandrasekaran, M. D. Tessier, D. Dupont, P. Geiregat, Z. Hens, E. Brainis, *Nano Lett.* **2017**, *17*, 6104.
[12] X. He, N. Ma, *Colloids Surf., B* **2014**, *124*, 118.
[13] T. Nann, W. M. Skinner, *ACS Nano* **2011**, *5*, 5291.
[14] H. M. Gil, T. W. Price, K. Chelani, J.-S. G. Bouillard, S. Calaminus, G. J. Stasiuk, *iScience* **2021**, *24*, 102189.
[15] M. D. Tessier, D. Dupont, K. De Nolf, J. De Roo, Z. Hens, *Chem. Mater.* **2015**, *27*, 4893.
[16] X. Michalet, F. F. Pinaud, L. A. Bentolila, J. M. Tsay, S. Doose, J. J. Li, G. Sundaresan, A. Wu, S. Gambhir, S. Weiss, *Science* **2005**, *307*, 538.
[17] S. Tamang, G. Beaune, I. Texier, P. Reiss, *ACS Nano* **2011**, *5*, 9392.
[18] K. D. Wegner, F. Dussert, D. Truffier-Boutry, A. Benayad, D. Beal, L. Mattera, W. L. Ling, M. Carrière, P. Reiss, *Front Chem* **2019**, *7*, 466.
[19] N. Zhan, G. Palui, H. Mattoussi, *Nat. Protoc.* **2015**, *10*, 859.
[20] T. Jin, F. Fujii, Y. Komai, J. Seki, A. Seiyama, Y. Yoshioka, *Int. J. Mol. Sci.* **2008**, *9*, 2044.
[21] R. Dunpall, A. A. Nejo, V. S. R. Pullabhotla, A. R. Opoku, N. Revaprasadu, A. Shonhai, *IUBMB Life* **2012**, *64*, 995.
[22] T.-Y. Lee, T. Jayakumar, P. Thanasekaran, K.-C. Lin, H.-M. Chen, P. Veerakumar, J.-R. Sheu, *Nanomaterials* **2020**, *10*, 1254.
[23] M. Allocca, L. Mattera, A. Bauduin, B. Miedziak, M. Moros, L. De Trizio, A. Tino, P. Reiss, A. Ambrosone, C. Tortiglione, *Environ. Sci. Technol.* **2019**, *53*, 3938.
[24] V. Brunetti, H. Chibli, R. Fiammengo, A. Galeone, M. A. Malvindi, G. Vecchio, R. Cingolani, J. L. Nadeau, P. P. Pompa, *Nanoscale* **2013**, *5*, 307.
[25] G. Lin, Q. Ouyang, R. Hu, Z. Ding, J. Tian, F. Yin, G. Xu, Q. Chen, X. Wang, K.-T. Yong, *Nanomed.: Nanotechnol. Biol. Med.* **2015**, *11*, 341.
[26] E. Yaghini, H. Turner, A. Pilling, I. Naasani, A. J. MacRobert, *Nanomed.: Nanotechnol. Biol. Med.* **2018**, *14*, 2644.
[27] Y. H. Suh, S. Lee, S. M. Jung, S. Y. Bang, J. Yang, X. B. Fan, S. Zhan, C. Samarakoon, J. W. Jo, Y. Kim, *Adv. Opt. Mater.* **2022**, *10*, 2102372.
[28] L. Pacchiarini, A. Tua, G. Grignani, *Haematologica* **1996**, *81*, 497.
[29] D. Mikhailidis, V. Fonseca, M. Barradas, R. Hutton, J. Jeremy, O. Epstein, N. McIntyre, P. Dandona, *Prostaglandins, Leukotrienes Essent. Fatty Acids* **1988**, *31*, 131.
[30] S. Matsuda, Y. Ikeda, M. Aoki, K. Toyama, K. Watanabe, Y. Ando, *Thromb Haemost* **1979**, *42*, 1324.
[31] D. W. Essex, M. Li, R. D. Feinman, A. Miller, *Blood* **2004**, *104*, 1383.
[32] T.-C. Chou, C.-Y. Shih, Y.-T. Chen, *J. Agric. Food Chem.* **2011**, *59*, 3050.
[33] Y.-S. Lai, C.-Y. Shih, Y.-F. Huang, T.-C. Chou, *J. Agric. Food Chem.* **2010**, *58*, 8596.
[34] D. P. Shepherd, K. J. Whitcomb, K. K. Milligan, P. M. Goodwin, M. P. Gelfand, A. Van Orden, *J. Phys. Chem. C* **2010**, *114*, 14831.
[35] C. Kagan, C. Murray, M. Nirmal, M. Bawendi, *Phys. Rev. Lett.* **1996**, *76*, 1517.
[36] K. F. Chou, A. M. Dennis, *Sensors* **2015**, *15*, 13288.
[37] J. R. Lakowicz, *Principles of fluorescence spectroscopy*, Springer, Boston, MA, USA **2006**.
[38] M. T. Montero, J. Hernández, J. Estelrich, *Biochem. Educ.* **1990**, *18*, 99.